Metabolism 168 (2025) 156262

Contents lists available at ScienceDirect

Metabolism

journal homepage: www.journals.elsevier.com/metabolism

Mechanical activation of adipose tissue macrophages mediated by Piezo1 protects against diet-induced obesity by regulating sympathetic activity

Shaoqiu Leng [a,b,1], Xiaoyu Zhang [a,b,1], Ruxia Zhao [a,1], Nan Jiang [a], Xinyue Liu [a], Xin Li [a], Qi Feng [a], Zi Sheng [a,c], Shuwen Wang [a,b,*], Jun Peng [a,b,c,**], Xiang Hu [a,b,*]

[a] Department of Hematology, Qilu Hospital of Shandong University, Jinan, China
[b] Shandong Key Laboratory of Hematological Diseases and Immune Microenvironment, Qilu Hospital of Shandong University, Jinan, China
[c] State Key Laboratory of Experimental Hematology, National Clinical Research Center for Blood Diseases, Institute of Hematology & Blood Diseases Hospital, Chinese Academy of Medical Sciences & Peking Union Medical College, Tianjin, China

ARTICLE INFO

Keywords:
Piezo1
Macrophage
Norepinephrine
Obesity
Slit3

ABSTRACT

Objective: Obesity-induced mechanical changes in white adipose tissue (WAT), including adipocyte hypertrophy and fibrosis, are hypothesized to alter adipose tissue macrophage (ATM) function through mechanosensitive pathways. This study aimed to determine whether the mechanosensor Piezo1 in ATMs regulates obesity-associated metabolic dysfunction and thermogenesis.

Methods: To investigate macrophage Piezo1 in obesity, myeloid-specific Piezo1-deficient mice (*Piezo1*$^{\Delta lyz2}$) and littermate controls (*Piezo1*$^{flox/+}$) were fed a high-fat diet (HFD) to induce obesity for 12 weeks. Metabolic assessments (GTT/ITT), tissue analyses (H&E staining, micro-CT), and RNA-seq were performed. Bone marrow transplantation and co-culture experiments (BMDMs with 3T3L1 adipocytes/PC12 neurons) were performed to evaluate macrophage-adipocyte/neuron crosstalk. Sympathetic activity was tested via cold exposure, NE measurement, and 6-OHDA/αMPT denervation. Molecular mechanisms were investigated using ChIP-qPCR.

Results: *Piezo1*$^{\Delta lyz2}$ mice exhibited aggravated HFD-induced obesity and insulin resistance despite reduced pro-inflammatory responses. Piezo1 deficiency in ATMs suppressed Slit3–ROBO1 signaling, leading to diminished NE secretion and impaired thermogenesis. Pharmacological inhibition of NE release (6-OHDA) or ROBO1 knockdown (shROBO1) abolished thermogenic disparities between *Piezo1*$^{\Delta lyz2}$ and control mice. Mechanistically, Piezo1 activation triggered SP1 nuclear translocation, directly binding to the Slit3 promoter to drive Slit3 transcription and secretion.

Conclusion: Piezo1 in ATMs mitigates obesity progression by promoting Slit3–ROBO1-dependent NE secretion and thermogenesis, independent of its pro-inflammatory role. This mechanosensitive pathway links WAT mechanical remodeling to metabolic regulation, which may offer a novel approach for managing obesity.

1. Introduction

Obesity, a global health concern linked to diseases such as type 2 diabetes, heart disease, and hypertension [1–5], arises from a chronic surplus of energy intake over expenditure, leading to excessive fat accumulation in adipose tissue. Adaptive thermogenesis, a major form of energy expenditure involving heat production in response to external stimuli such as cold and nutrition, is a pivotal process [6–9]. Adipose tissue is categorically divided into white adipose tissue (WAT), responsible for energy storage, and brown adipose tissue (BAT), which dissipates energy as heat [10–12]. Furthermore, brown-like adipocytes, also referred to as beige adipose tissue, appear scattered within WAT under continuous external stimulation [13–16]. Mitochondrial uncoupling protein 1 (UCP1), located in the inner mitochondrial transmembrane, aids in uncoupling oxidative phosphorylation to generate heat, and therefore, is a vital effector protein for the function of BAT and beige

* Corresponding authors at: Shandong Key Laboratory of Immunochematology, Qilu Hospital, Cheeloo College of Medicine, Shandong University, Jinan, China.
** Corresponding author at: Department of Hematology, Qilu Hospital, Cheeloo College of Medicine, Shandong University, Jinan, China.
E-mail addresses: 15066693988@163.com (S. Wang), junpeng88@sina.com.cn (J. Peng), huxiang08@sina.com (X. Hu).
[1] Shaoqiu Leng, Xiaoyu Zhang and Ruxia Zhao contributed equally to this study.

https://doi.org/10.1016/j.metabol.2025.156262
Received 12 November 2024; Accepted 3 April 2025
Available online 7 April 2025

adipose tissue [17–20]. However, during obesity, the mechanism underlying alterations in metabolic, endocrine, and thermogenic functions in adipose tissue, coinciding with mechanical properties of the microenvironment, remain poorly understood, limiting the development of targeted therapies for obesity and associated metabolic complications.

Adipose tissue comprises adipocytes, stromal cells, and immune cells, including macrophages. Adipose tissue macrophages (ATMs), which are mainly derived from infiltrating monocytes, account for approximately 5 % of the stromal vascular fraction (SVF) in the lean state, but up to 50 % during obesity [21]. These macrophages can be categorized as pro-inflammatory (M1) or anti-inflammatory (M2) [22–25].Obesity tends to polarize ATMs toward the pro-inflammatory M1 state, contributing to adipose tissue inflammation by upregulating pro-inflammatory and pro-coagulant proteins such as tumor necrosis factor-alpha (TNF-α), interleukin-6 (IL-6), inducible nitric oxide synthase (iNOS), monocyte chemotactic protein-1 (MCP-1), and plasminogen activator (PA), which have implications for the metabolic complications of obesity. Conversely, M2 polarization of ATMs is associated with an anti-inflammatory phenotype, potentially aiding inflammation resolution and insulin sensitivity [26–30].

Beyond their inflammatory roles, ATMs are involved in regulating obesity-related hormones. Norepinephrine (NE), released from sympathetic nerves, governs adaptive thermogenesis in adipose tissue. ATMs can uptake and degrade NE via the expression of solute carrier family 6 member 2 (SLC6A2) and monoamine oxidase A (MAOA), thereby reducing the local NE levels [31]. Additionally, Wang et al. reported that ATMs can promote sympathetic activity and mitigate obesity by secreting Slit3 [32]. However, understanding the dynamic regulation of NE by ATMs during obesity with complex mechanical characteristics remains a challenge.

Obesity triggers excessive energy storage, resulting in adipose tissue remodeling, an inflammatory microenvironment, adipose tissue fibrosis, and increased extracellular matrix accumulation [33]. These processes induce significant mechanical changes and physical space constraints, likely perpetuating a constitutively activated mechanosensation signal within adipose tissue [34]. Mechanosensitive ion channels (MSICs), which sense mechanical forces and initiate mechanosensitive signal transduction, play critical roles in both normal physiology and pathological conditions. Among these channels, Piezo1, a recently discovered mechano-activated ion channel with a high affinity for calcium ions, is of particular significance [35–38]. In obese mice, mature adipocytes lacking Piezo1 demonstrated a reduced secretion of adipogenic fibroblast growth factor 1 (FGF1), failing to induce pre-adipocyte differentiation [39]. Furthermore, adipocyte-specific Piezo1 knockout mice exhibit altered expression of pro-inflammatory and lipolysis genes in adipose tissue, resulting in insulin resistance when subjected to a high-fat diet (HFD) [40]. While the role of Piezo1 in adipocytes is well-established, its impact on ATMs function remains unexplored, limiting our full insights of the regulation to adipose tissue by mechanical forces during obesity.

Previous reports had consistently linked Piezo1 to an enhanced pro-inflammatory macrophage phenotype, and we hypothesized that Piezo1 deficiency in ATMs would reduce inflammation and ameliorate obesity [35,37,41]. To validate our hypothesis, we generated transgenic mice with specific Piezo1 deficiency in macrophages and subjected them to an HFD challenge. But surprisingly, our results demonstrated that Piezo1 deficiency in ATMs of obese mice caused an increased body weight and more severe insulin resistance. Mechanistically, Piezo1 deficiency in ATMs limits the host thermogenesis by decreasing NE secretion from sympathetic nerves, and thus results in an impaired energy expenditure. Here, we uncovered an unexpected association between mechanosensation and the neuro-regulatory role of ATMs in obesity and proposed the self-limiting mechanism of ATMs to maintain adipose tissue stability, which advances the understanding of obesity and inspires new treatment strategies.

2. Methods

2.1. Ethics statement

Approval for animal experiments was granted by the Animal Ethics Committee of Cheeloo College of Medicine, Shandong University.

2.2. Animals

The mice involved in this study were housed in a Specific Pathogen-Free (SPF) facility, where environmental conditions were controlled to maintain a temperature range of 21.5–23 °C, a 12-h light-dark cycle, humidity levels between 40 and 60 %, and provision of irradiated food and water tailored to meet the specific experimental requirements). During the experiments conducted at room temperature, mice were put in the caged exposed to room air, whereas they were placed within cages situated inside temperature-controlled chambers for experiments at 4 °C. The mice strains used in this study, namely B6.Cg-Piezo1$^{tm2.1Apat}$/J (JAX Stock No: 029213, *Piezo1*$^{flox/flox}$) and B6;129S6-Polr2a$^{Tn(pb\text{-}CAG\text{-}GCaMP5g)Tvrd}$/J (JAX Stock No: 024477, PC-G5) were obtained from the Jackson Laboratory; *Lyz2*^{cre} mice were kindly provided by Prof. Qi Xiaopeng from Shandong University. To generate myeloid Piezo1 conditional deficient mice, *Piezo1*$^{flox/flox}$ and *Lyz2*^{cre} mice were crossed. Genotype analysis was performed using the following primers:

Piezo1$^{flox/flox}$:

P1, 5′-GCC TAG ATT CAC CTG GCT TC-3′; P2, 5′-GCT CTT AAC CAT TGA GCC ATC T-3′;

Lyz2^{cre}:

P1, 5′-CCC AGA AAT GCC AGA TTA CG-3′; P2, 5′-CTT GGG CTG CCA GAA TTT CTC-3′.

PC-G5:

P1, 5′- TAG ACA CAT GCC ACC AAA CC-3′; P2, 5′- TCT CTC CAG CAC CAT AAC TCC-3′; P3, 5′- GAT CGA TAA AAC ACA TGC GTC A-3′.

For in vivo treatment, bilateral injections of 6-OHDA (MedChemExpress) were administered into the fat pad at a dosage of 400 μg per lobe. Bilateral αMPT (MedChemExpress) injections were delivered into the adipose tissue at 125 mg/kg body weight per lobular region. Lentivirus was constructed by Shanghai Genechem Co., Ltd., and detailed target sequences are provided in Supplementary Table 1. The 1×10^9 shCtrl or shRobo1 solution was injected into the bilateral fat pads thrice weekly.

2.3. Cell culture

To induce the differentiation of bone marrow-derived macrophages (BMDMs), mice with specific genotypes were euthanized through continued exposure to isoflurane (5 %) for 1 min after respiratory arrest. Sterile cells were harvested from the femurs and tibias and red blood cells were lysed using a lysis buffer. The resulting single-cell bone marrow suspension was filtered through 70-μm cell filters and cultured in complete Dulbecco's modified Eagle medium (DMEM) conditioned medium containing 50 ng mL^{-1} recombinant mouse M-CSF (PeproTech) to facilitate BMDM differentiation. The *Rattus norvegicus* pheochromocytoma PC12 cell line was cultured in RPMI-1640 medium (Gibco) supplemented with 10 % heat-inactivated horse serum (Solarbio), 5 % FBS (Gibco), and 1 % penicillin/streptomycin solution. For PC12 differentiation, the cells were cultured with nerve growth factor (PeproTech) for 5 days. For preadipocytes differentiation, mouse 3 T3-L1 cells were cultured in DMEM supplemented with 10 % calf serum (Pricella) and 1 % penicillin/streptomycin solution until they reached confluence (day 0). Subsequently, the cells were cultured in a lipogenic induction medium containing methylisobutylxanthine (520 μmol L^{-1}), dexamethasone (1 μmol L^{-1}), and insulin (167 nmol L^{-1}) for 2 days, followed by replacement of the medium with a lipogenic maintenance medium containing 167 nmol L^{-1} insulin.

2.4. SVFs isolation and magnetic bead sorting

After euthanasia, approximately 3–5 g of adipose tissue was collected from each mouse and placed in cold medium. Subsequently, blood vessels and fibers were removed from the adipose tissue, which was then cut into small pieces. An equal volume of type II collagenase was added, and the mixture was digested at 37 °C for 30 min until the particles disappeared. Digestion was quenched by adding the same volume of complete culture medium. The cell suspension obtained was filtered through a strainer, and after liquid stratification, the upper layer consisted of adipose cells, the middle layer contained SVFs, and the bottom layer consisted of undigested fibrous tissues. The cell suspension in the middle layer was aspirated, and red blood cells were subsequently removed. Following centrifugation, cells were resuspended in phosphate-buffered saline (PBS) for magnetic bead separation or flow analysis.

For cell sorting, SVFs were resuspended in 1 mL 1× MojoSort Buffer Solution (Miltenyi Biotec), filtered, and centrifuged. The cell pellets were resuspended with 90 μL 1× MojoSort Buffer Solution and 10 μL F4/80-biotin antibody (Miltenyi Biotec) for 15 min. The staining was terminated by adding 1× MojoSort Buffer Solution. After centrifugation, 1 mL of 1× MojoSort Buffer Solution was added to resuspend the cells, and the cell suspension was placed on a magnetic bead-sorting MS column for sorting.

2.5. HFD-induced obesity model

The mice were subjected to either HFD (D12492) containing 60 % fat or a normal chow diet (LFD) (D12450B) from 8 weeks of ages. The mice were placed in a 12-h light-dark cycle and provided with ad libitum access to food and water. Body weight was monitored and recorded weekly.

2.6. RNA extraction and real-time quantitative polymerase chain reaction (RT-qPCR)

Animal tissues were frozen in liquid nitrogen and RNA was extracted from lysed cells or tissues using TRIzol reagent (Invitrogen). mRNA was reverse-transcribed into cDNA using the Prime Script RT kit (Takara Bio Inc.), following the manufacturer's instructions. mRNA levels were quantified using the TM SYBR Green PCR Kit (Takara Bio Inc.), and data were acquired using the Light Cycler 480 system (Roche Applied Sciences). Allele-specific primers are provided in Supplementary Table 2.

2.7. Protein extraction and western blotting

For western blotting, cultured cells were collected and washed twice with PBS. Protein was extracted using protein extraction kits (BestBio) according to the manufacturer's instructions. The protein concentration was determined using the BCA protein assay kit, followed by SDS-PAGE separation. The separated proteins were transferred to polyvinylidene fluoride (PVDF) membranes (MilliporeSigma). Subsequently, the membranes were incubated with the primary antibody (1:1000) at 4 °C overnight, washed on the following day, and incubated with the secondary antibody for 1 h.

The following commercial antibodies were used:

Rabbit anti-mouse UCP1 (Abcam, Ab234430)
Rabbit anti-mouse ATGL (Abclonal, A5126)
Rabbit anti-mouse HSL (Abclonal, A15686)
Rabbit anti-mouse p-HSL (Abclonal, AP1151)
Rabbit anti-mouse TH (Abclonal, A5079)
Rabbit anti-mouse p-TH (Abclonal, AP0210)
Rabbit anti-mouse MAOA (Abacm, Ab126751)
Rabbit anti-mouse SLIT3 (RD, AF3629)
Rabbit anti- mouse ROBO1 (Abcam, Ab7279)
HRP-conjugated β-actin monoclonal (Proteintech, HRP-60008)
HRP goat anti-rabbit IgG (Abclonal, AS014)

2.8. Glucose tolerance test (GTT)

Wild-type (*Piezo1*$^{fl/+}$) and conditional knockout (*Piezo1*$^{\Delta lyz2}$) mice that had been subjected to either LFD or HFD induction were fasted overnight. The following day, mice were weighed, and blood was collected from tail clippings for measurement of fasting blood glucose levels. Subsequently, mice were intraperitoneally injected with a 2 g/kg glucose solution (Sigma), and blood glucose values were recorded at 15, 30, 60, and 120 min post-injection for subsequent data analysis using blood glucose meter (Sinocare).

2.9. Insulin tolerance test (ITT)

Piezo1$^{fl/+}$ and *Piezo1*$^{\Delta lyz2}$ mice that had undergone LFD or HFD induction were subjected to a 4–6 h fasting period. On the subsequent day, mice were weighed, and blood was collected from tail clippings for measurement of fasting blood glucose levels. Mice were intraperitoneally injected with 0.75 IU/kg insulin solution, and blood glucose values were recorded at 15, 30, 60, and 120 min post-injection. All experimental data were recorded and analyzed accordingly.

2.10. ATMs transplantation experiment

Recipient mice were provided with antibiotic-treated water for 2 days prior to irradiation with a lethal dose. Three hours after irradiation, 2×10^6 whole-bone marrow cells from *Piezo1*$^{fl/+}$ and *Piezo1*$^{\Delta lyz2}$ mice were transplanted for reconstruction. For transplantation experiments following lentiviral treatment, first, 2×10^6 whole bone marrow cells were aseptically isolated, then infected with lentivirus in vitro for 24 h prior to transplantation. Following reconstruction, mice were fed LFD or HFD, and their weights were monitored weekly. After 12 weeks, glucose metabolism indices were assessed.

2.11. Immunofluorescence and immunohistochemistry

Tissues isolated from the mice were fixed in 4 % paraformaldehyde for 24 h at room temperature. These tissues were subsequently embedded in paraffin and sectioned at 5-μm thickness. Before staining, sections underwent deparaffinization and rehydration using graded concentrations of ethanol. Sections were then subjected to staining with primary antibodies overnight at 4 °C. Following washing, tissue sections were incubated with secondary antibodies (1:1000), and images were captured using confocal microscopy.

2.12. RNA-seq

RNA-seq data analysis was conducted by BGI company. The mRNA library was prepared, and data filtering was performed using SOAPnuke (v1.5.6). The filtering process included the removal of reads containing joints to prevent joint contamination, reads with unknown base N content exceeding 5 %, and low-quality reads, resulting in clean data. The Dr. Tom Multiomics Data Mining System (https://biosys.bgi.com) was used for subsequent data analysis. RSEM software facilitated gene expression quantification by comparing clean data with the reference genome and reference gene sets. Pheatmap was utilized to generate expression clustering heatmaps. DEGseq was employed for differential gene detection, with differences with Q value <0.05 selected for enrichment analysis. The first 1000 differentially ranked genes were selected, and Phyper was used for enrichment analysis based on a hypergeometric test.

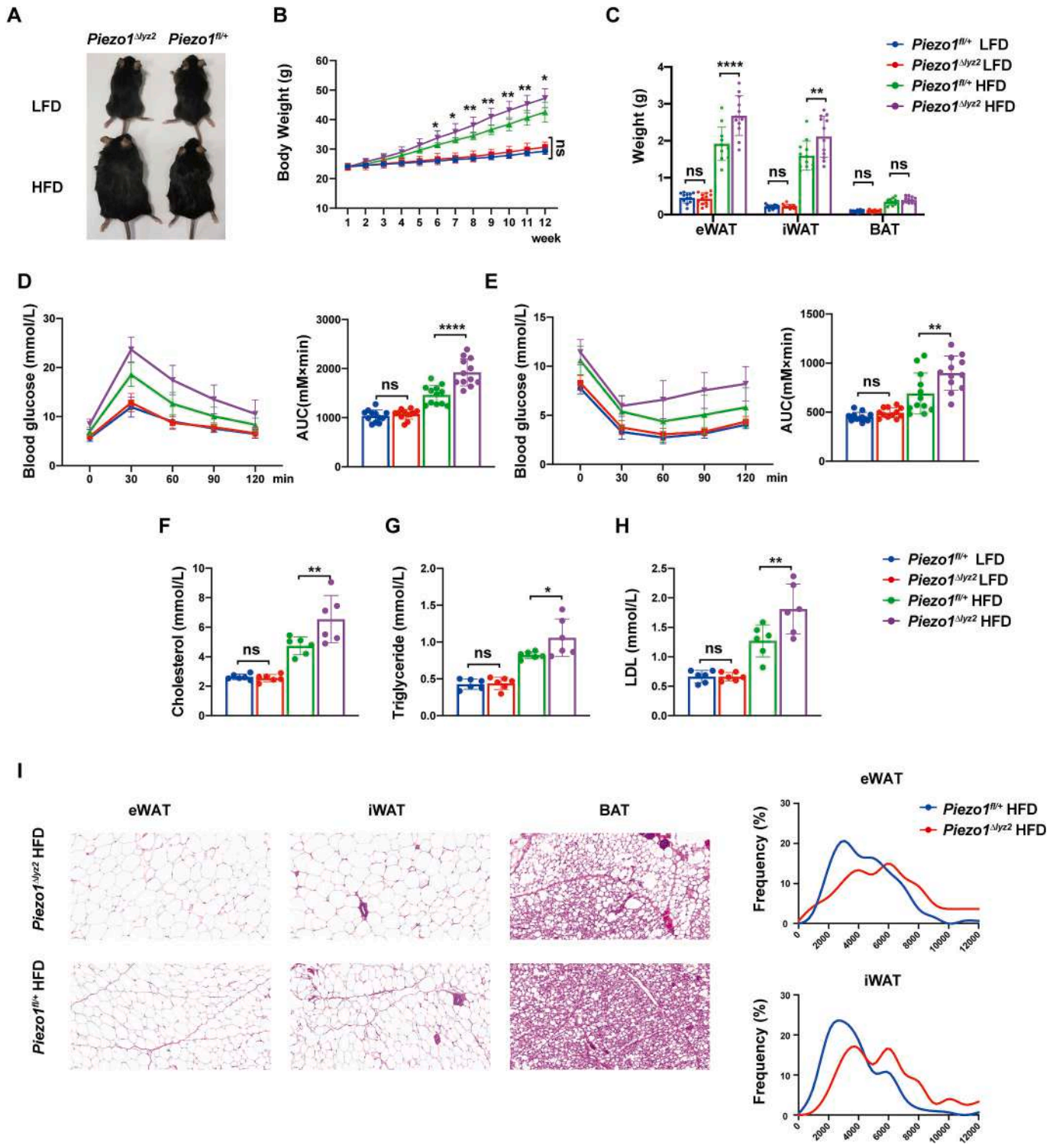

Fig. 1. Piezo1 deficiency in macrophages sensitizes mice to obesity.
(**A**) Representative images of *Piezo1*$^{flox/+}$ and *Piezo1*$^{\Delta lyz2}$ mice subjected to either HFD or LFD for 12 weeks. (**B**) Body weight records for *Piezo1*$^{flox/+}$ and *Piezo1*$^{\Delta lyz2}$ mice exposed to HFD or LFD for 12 weeks ($n = 12$ mice per group). (**C**) Quantification of fat pads in *Piezo1*$^{flox/+}$ and *Piezo1*$^{\Delta lyz2}$ mice after 12 weeks on HFD or LFD (n = 12 mice per group). (**D**, **E**) GTT and ITT of *Piezo1*$^{flox/+}$ and *Piezo1*$^{\Delta lyz2}$ mice on HFD or LFD for 12 weeks (n = 12 mice per group) (**F–H**) Serum lipid indices (cholesterol, triglycerides, LDL) in *Piezo1*$^{flox/+}$ and *Piezo1*$^{\Delta lyz2}$ mice under HFD or LFD conditions for 12 weeks ($n = 6$ mice per group). (**I**) Representative H&E images and quantification of adipocyte diameter in eWAT, iWAT, and BAT in *Piezo1*$^{flox/+}$ and *Piezo1*$^{\Delta lyz2}$ mice after 12 weeks on HFD (total 300 cells per group). Data are expressed as the mean ± SD. Statistical significance was assessed using (**B**) two-way ANOVA, $^{*}P < 0.05$, $^{**}P < 0.01$, ns = not significant, and (**C–H**) one-way ANOVA, Tukey's multiple comparisons test, $^{*}P < 0.05$, $^{**}P < 0.01$, $^{****}P < 0.0001$, ns = not significant.
HFD, high-fat diet; LFD, low-fat diet; eWAT, epididymal white adipose tissue; iWAT, inguinal white adipose tissue; BAT, brown adipose tissue; GTT, glucose tolerance test; ITT, insulin tolerance test. (For interpretation of the references to color in this figure legend, the reader is referred to the web version of this article.)

2.13. ScRNA-seq analysis

The single-cell RNA sequencing (scRNA-seq) dataset analyzed in this study was acquired from the Gene Expression Omnibus (GEO) database (GSE156110), with a focused selection of human adipose tissue macrophage populations from two distinct metabolic states: adipose tissue macrophages derived from the lean donor (GSM4724867) and those obtained from the obese donor (GSM4724868) for subsequent bioinformatic analysis. The scRNA-seq data processing pipeline was implemented using the Seurat R package. Initial quality control involved exclusion of cells demonstrating >10 % mitochondrial gene content or <500 uniquely expressed genes. Perform integration by FindIntegrationAnchors and IntegrateData, and then scale features in the dataset. Cell clustering was performed employing graph-based clustering (resolution = 0.1) with subsequent dimensionality reduction visualization via t-distributed stochastic neighbor embedding (t-SNE).

2.14. Metabolic cage study

An animal high-throughput metabolic analysis system (OXYMAX-CLAMS, Columbus Instruments) was preheated and used for metabolic cage study. The mice were individually housed in metabolic cages and acclimated for 24 h before initiating the experiment to minimize stress. The system automatically recorded physiological parameters of the experimental mice over a period of 72 h. These parameters included food intake, activity, oxygen consumption (VO2, mL/kg/h), energy consumption (heat production rate, kcal/h), and respiratory exchange rate. Data analysis was conducted post-experiment.

2.15. Lipid profile assays

Serum samples were stored at −80 °C until further use. Assay kits (Jiancheng Bioengineering Institute) were utilized to measure serum levels of triglycerides (TG), cholesterol, high-density lipoprotein (HDL), and LDL following the recommended protocol.

2.16. Elisa

A mouse noradrenaline (NA) ELISA Kit (Elabscience) was used to determine NE levels, following the manufacturer's recommended procedure. The Slit3 ELISA Kit (Cloud-Clone Corp.) was used to detect Slit3 levels according to the recommended procedure.

2.17. Transcription factor prediction

Online softwares were used to predict the transcription factors that bind to the 2000-bp promoter sequence of mouse Slit3 gene. Use the PROMO (http://alggen.lsi.upc.es/), TFDB (https://guolab.wchscu.cn/AnimalTFDB/) and GTRD (http://gtrd.biouml.org.) to predict the transcription factors that may be bound to promoter sequence of Slit3, the error tolerance rate in PROMO was set to 5 %.

2.18. ChIP-qPCR

Chromatin immunoprecipitation (ChIP) was performed using the SimpleChIP® Plus Enzymatic Chromatin IP Kit (CST) according to the manufacturer's protocols. Briefly, samples were crosslinked with 1 % formaldehyde (final concentration) under optimized conditions. Following crosslinking, cells were lysed using Cell Swelling Buffer and subjected to chromatin fragmentation via ultrasonication in Sonication Buffer. After sonication, 5 % of the fragmented chromatin from each sample was reserved as Input controls. The remaining chromatin was divided into aliquots for immunoprecipitation (IP) using either Sp1-specific antibody or normal IgG (negative control). Post-IP, chromatin-antibody complexes were eluted with ChIP Elution Buffer and subjected to reversal of crosslinks. DNA was subsequently purified and analyzed by PCR amplification.

2.19. Statistical analysis

Experimental data are presented as mean ± standard deviation. Normality tests were performed using the Shapiro–Wilk test. Group comparisons were performed using one-way ANOVA, two-way ANOVA, or unpaired two-tailed Student's *t*-test. Statistical significance was set at $P < 0.05$.

3. Results

3.1. Piezo1 deficiency in macrophages sensitizes mice to obesity

To assess the function of Piezo1 specifically in macrophages during obesity, we generated myeloid-specific Piezo1-deficient transgenic mice by crossing *Lyz2*^{cre} and *Piezo1*$^{flox/flox}$ mice. *Lyz2*^{cre} *Piezo1*$^{flox/flox}$ (*Piezo1*$^{\Delta lyz2}$) and sex-matched littermate *Piezo1*$^{flox/+}$ mice were fed either a LFD or HFD from 8 weeks of ages for up to 12 weeks. Counterintuitively, *Piezo1*$^{\Delta lyz2}$ mice exhibited increased weight gain when subjected to the HFD, whereas the weight did not significantly differ between the two groups of mice on LFD (Fig. 1A, B). Correspondingly, *Piezo1*$^{\Delta lyz2}$ mice displayed higher WAT mass compared with that in *Piezo1*$^{flox/+}$ mice (Fig. 1C), which was confirmed using micro computed tomography (micro-CT) (Supplementary Fig. 1A). Whether female or male mice, the *Piezo1*$^{\Delta lyz2}$ group showed a higher body weight increase compared with *Piezo1*$^{flox/+}$ group, indicating that the effect of Piezo1 on body weight is independent of gender (Supplementary Fig. 1B). As obesity can lead to glucose intolerance and insulin resistance, we examined the impact of myeloid Piezo1 on glucose homeostasis and insulin sensitivity. GTT and ITT results indicated that myeloid Piezo1 did not affect glucose homeostasis in LFD-fed mice. However, HFD-fed *Piezo1*$^{\Delta lyz2}$ mice exhibited more severe glucose intolerance and insulin resistance relative to HFD-fed *Piezo1*$^{flox/+}$ mice (Fig. 1D, E). Furthermore, *Piezo1*$^{\Delta lyz2}$ mice displayed elevated plasma cholesterol, triglyceride, and low-density lipoprotein (LDL) levels upon HFD challenge (Fig. 1F–H). Collectively, Piezo1 deficiency in macrophages worsened obesity progression and metabolic imbalances.

Additionally, H&E staining of adipose tissue revealed larger adipocytes in epidermal WAT (eWAT, visceral) and inguinal WAT (iWAT, subcutaneous) in HFD-fed *Piezo1*$^{\Delta lyz2}$ mice (Fig. 1I). However, the adipose tissue pathology did not significantly differ in LFD-fed mice (Supplementary Fig. 1C). HFD-fed *Piezo1*$^{\Delta lyz2}$ mice also exhibited increased lipid accumulation in liver sections, as visualized using oil red staining (Supplementary Fig. 1D). Furthermore, the *Piezo1*$^{\Delta lyz2}$ mice displayed compensatory hypertrophy of the islets (Supplementary Fig. 1E).

Furthermore, to evaluate Piezo1 expression in human ATMs, we analyzed single-cell sequencing data from the publicly available dataset [42]. By examining Piezo1 expression in sorted ATMs from lean or obese donor, we observed a significant elevation of Piezo1 levels in macrophages from obese adipose tissue. This finding suggests that Piezo1 expression in human adipose tissue macrophages may play a critical role in regulating adipose tissue homeostasis (Supplementary Fig. 1F).

3.2. Myeloid Piezo1 enhances energy expenditure and adaptive thermogenesis

Given the more pronounced body weight changes observed in male mice under high-fat diet conditions and their insensitivity to fluctuations in estrogen and progesterone levels, we chose male mice for subsequent experiments. To elucidate the mechanism behind the significantly increased fat storage in HFD-fed *Piezo1*$^{\Delta lyz2}$ mice, we employed metabolic cages to assess food intake, physical activity (wheel counts), heat production, and O_2 consumption in *Piezo1*$^{flox/+}$ and *Piezo1*$^{\Delta lyz2}$ mice. No significant differences were observed in food intake, wheel counts, O_2 consumption, or heat production between the two groups of LFD-fed

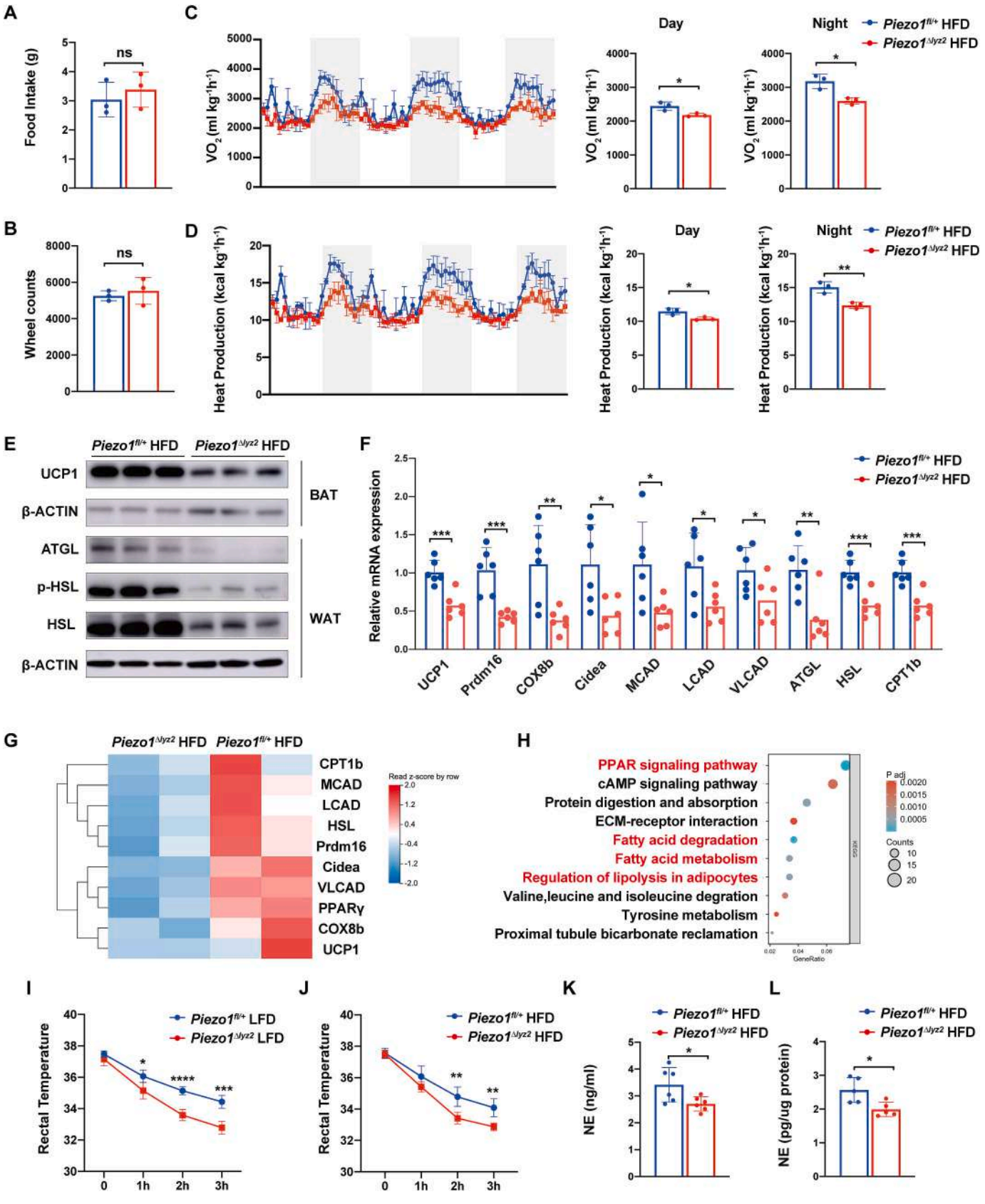

(caption on next page)

Fig. 2. Myeloid Piezo1 enhances energy expenditure and adaptive thermogenesis.
(**A**) Measurements of food intake, (**B**) wheel counts, (**C**) oxygen consumption, and (**D**) heat production in *Piezo1*$^{flox/+}$ and *Piezo1*$^{\Delta lyz2}$ mice challenged with HFD as determined by metabolic cages ($n = 3$ mice per group). (**E**) Protein expression analysis of UCP1, ATGL, p-HSL, and t-HSL in adipose tissue (n = 3 mice per group). (**F**) qPCR analysis of mRNA levels for genes related to thermogenesis and lipolysis WAT isolated from *Piezo1*$^{flox/+}$ and *Piezo1*$^{\Delta lyz2}$ mice fed with HFD (n = 6 mice per group). (**G**) Heat map illustrating lipid metabolism-related genes based on the normalized read count of genes in WAT samples from *Piezo1*$^{flox/+}$ and *Piezo1*$^{\Delta lyz2}$ mice challenged with HFD. (**H**) KEGG pathway enrichment analysis of genes downregulated in adipose tissue from *Piezo1*$^{\Delta lyz2}$ mice ($Log_2FC > 0.5$, Padj<0.05). (**I, J**) Rectal temperature measurements for *Piezo1*$^{flox/+}$ and *Piezo1*$^{\Delta lyz2}$ mice on LFD or HFD subjected to a 4 °C cold challenge for 180 min (n = 6 mice per group). (**K**) NE levels in the serum of *Piezo1*$^{flox/+}$ and *Piezo1*$^{\Delta lyz2}$ mice challenged with HFD (n = 6 mice per group). (**L**) NE levels in the WAT of *Piezo1*$^{flox/+}$ and *Piezo1*$^{\Delta lyz2}$ mice challenged with HFD (n = 6 mice per group). Statistical significances were calculated using (**I, J**) Two-way ANOVA and Tukey's multiple comparisons test and (**A–D, F, K, L**) two-tailed Student *t*-test. Data are expressed as the mean ± SD. *P < 0.05, **P < 0.01, ***P < 0.001; **** P < 0.0001, ns = not significant.
HFD, high-fat diet; LFD, low-fat diet; WAT, white adipose tissue; KEGG, Kyoto Encyclopedia of Genes and Genomes; NE, Norepinephrine.

mice (Supplementary Fig. 2 A-D). HFD feeding did not induce significant differences in food intake (Fig. 2A) or wheel counts (Fig. 2B). However, O_2 consumption (Fig. 2C) and heat production (Fig. 2D) were markedly decreased in HFD-fed *Piezo1*$^{\Delta lyz2}$ mice during both dark and light phases compared with that in *Piezo1*$^{flox/+}$ mice.

Energy expenditure is often accompanied by increased lipolysis and heat production. Protein expression analysis of UCP1 in BAT and key lipid metabolic genes, including ATGL, p-HSL, and HSL, in WAT revealed decreased expression in the adipose tissue of HFD-fed *Piezo1*$^{\Delta lyz2}$ mice compared to littermate controls (Fig. 2E, Supplementary Fig. 2E). Furthermore, mRNA expression of key thermogenic genes such as UCP1, Prdm16, COX8b, and Cidea, and key lipid metabolic genes, such as MCAD, LCAD, VLCAD, ATGL, HSL, and CPT1b, was reduced in the WAT of HFD-fed *Piezo1*$^{\Delta lyz2}$ mice (Fig. 2F). RNA sequencing of isolated WAT corroborated these findings, with the clustering heat map indicating downregulated expression of genes associated with lipolysis and thermogenesis in *Piezo1*$^{\Delta lyz2}$ mice, suggesting impaired thermogenic function of adipose tissue (Fig. 2G). Moreover, genes downregulated in adipose tissue with Piezo1-deficient ATMs were enriched in fatty acid metabolism-related pathways, including the peroxisome proliferator-activated receptor (PPAR) signaling pathway, fatty acid degradation, fatty acid metabolism, and regulation of lipolysis in adipocytes (Fig. 2H and Supplementary Fig. 2F).

Given the evidence of altered heat production in HFD-fed *Piezo1*$^{\Delta lyz2}$ mice, we examined cold-induced adaptive thermogenesis. When mice were exposed to 4 °C from room temperature, rectal temperature dropped in both *Piezo1*$^{flox/+}$ and *Piezo1*$^{\Delta lyz2}$ mice, but the drop was considerably more significant in *Piezo1*$^{\Delta lyz2}$ mice, whether on an LFD or HFD (Fig. 2I, J). LFD-fed *Piezo1*$^{\Delta lyz2}$ mice exhibited a weaker thermogenic response to cold stimulation, despite no difference in body weight relative to *Piezo1*$^{flox/+}$ mice. As adaptive thermogenesis is strictly regulated by the sympathetic nervous system, with Norepinephrine (NE) as its principal effector [43], we measured NE levels in both serum and adipose tissue. Concordantly, *Piezo1*$^{\Delta lyz2}$ mice exhibited reduced NE levels in both plasma and adipose tissue (Fig. 2K, L). Given that epinephrine is also a core effector molecule of the sympathetic nervous system and can induce systemic stress responses through circulation, we subsequently measured epinephrine levels in plasma and adipose tissue. The results showed no significant differences between *Piezo1*$^{flox/+}$ and *Piezo1*$^{\Delta lyz2}$ mice in either plasma or adipose tissue under obese conditions (Supplementary Fig. 2G, H). Notably, since sympathetic nerve terminals in adipose tissue exclusively release NE, epinephrine levels in adipose tissue were extremely low and nearly below the detection limit. These findings suggest that Piezo1 deficiency in macrophages may regulate the development of obesity by affecting NE levels.

3.3. The adipose tissue macrophages are imperative in body weight regulation with HFD challenge

As Piezo1 is a mechanically sensitive calcium ion channel, we designed experiments to investigate whether Piezo1 is activated in ATMs. Given the difficulty of directly measuring mechanical stress changes in local macrophages in situ, we indirectly assessed the functional activity of Piezo1 by monitoring calcium ion influx strength. We crossed *Lyz2*^{cre} *Piezo1*$^{flox/flox}$ and PC-G5, and generated Cre-induced transgenic reporter mice expressing the fluorescent calcium indicator protein GCaMP5G variant in macrophages, both with and without Piezo1 knockout (Fig. 3A). In these fluorescent reporter mice, increased intracellular calcium levels results in bright green fluorescent protein (GFP) fluorescence in Lyz2-expressing cells. Consistent with previous findings, after 3 months of being fed a low-fat diet, there were no significant differences in body weight and glucose tolerance between *Piezo1*$^{flox/+}$ and *Piezo1*$^{\Delta lyz2}$ mice (Supplementary Fig. 3A–C). While, *Piezo1*$^{\Delta lyz2}$ mice with the GCaMP5G variant displayed increased weight gain, exacerbated glucose intolerance, and larger fat cell sizes after HFD feeding (Supplementary Fig. 3D–G). Quantitative analysis revealed weak calcium reporter fluorescence in both *Piezo1*$^{flox/+}$ and *Piezo1*$^{\Delta lyz2}$ mice on a low-fat diet, with no intergroup differences. However, obesity induction triggered a significant fluorescence increase in *Piezo1*$^{flox/+}$ ATMs, which was absent in *Piezo1*$^{\Delta lyz2}$ mice (Fig. 3B, C). These results suggested that Piezo1 plays a major role in mediating intracellular calcium ion influx in ATMs during the development of obesity owing to mechanical changes within the enlarged adipose tissue.

Macrophages are distributed throughout the body and arise from two distinct lineages: tissue-resident macrophages, capable of local self-renewal independently of adult hematopoiesis, and monocyte-derived macrophages, primarily originating from adult hematopoietic stem cells and recruited to sites of inflammation [44–48]. Considering the weaken calcium influx of ATMs observed in conditioned knockout mice on HFD, we investigated whether Piezo1 deficiency was linked to changes in the hematopoietic compartment. We transplanted bone marrow from *Piezo1*$^{flox/+}$ and *Piezo1*$^{\Delta lyz2}$ litters into wild-type mice, maintaining either an HFD or LFD after transplantation (Fig. 3D). We observed no significant difference in body weight between the two groups of LFD-fed mice. However, recipients of *Piezo1*$^{\Delta lyz2}$ bone marrow displayed higher weight gain when exposed to an HFD (Fig. 3E). Concordantly, H&E staining of adipose tissue revealed larger adipocytes in eWAT and iWAT in recipients of *Piezo1*$^{\Delta lyz2}$ bone marrow transplants subjected to the HFD challenge (Supplementary Fig. 3H). GTT and ITT results confirmed the lack of difference in glucose homeostasis between the two groups of LFD-fed mice (Fig. 3F–G), whereas recipients of *Piezo1*$^{\Delta lyz2}$ bone marrow transplantation displayed more severe glucose intolerance and insulin resistance after HFD feeding (Fig. 3H–I). These findings suggest that Piezo1 deficiency in monocyte-derived ATMs may primarily influence the metabolic imbalance in HFD-challenged *Piezo1*$^{\Delta lyz2}$ mice.

3.4. Myeloid Piezo1 regulates weight gain and glucose tolerance in sympathetic activity-dependent pathway

Subsequently, we conducted in vitro experiments to investigate whether Piezo1 activation in ATMs affects adipocytes or sympathetic nerve cells. We co-cultured *Piezo1*$^{flox/+}$ and *Piezo1*$^{\Delta lyz2}$ BMDMs with 3T3L1 adipocytes. There was no significant difference in ATGL, p-HSL and HSL of adipocytes co-cultured with *Piezo1*$^{flox/+}$ and *Piezo1*$^{\Delta lyz2}$ macrophages (Fig. 4A, Supplementary Fig. 4A). We then used Yoda1, a chemical agonist of Piezo1, to stimulate BMDMs to mimic the activation of macrophages in adipose tissue, followed by co-culture with 3T3L1

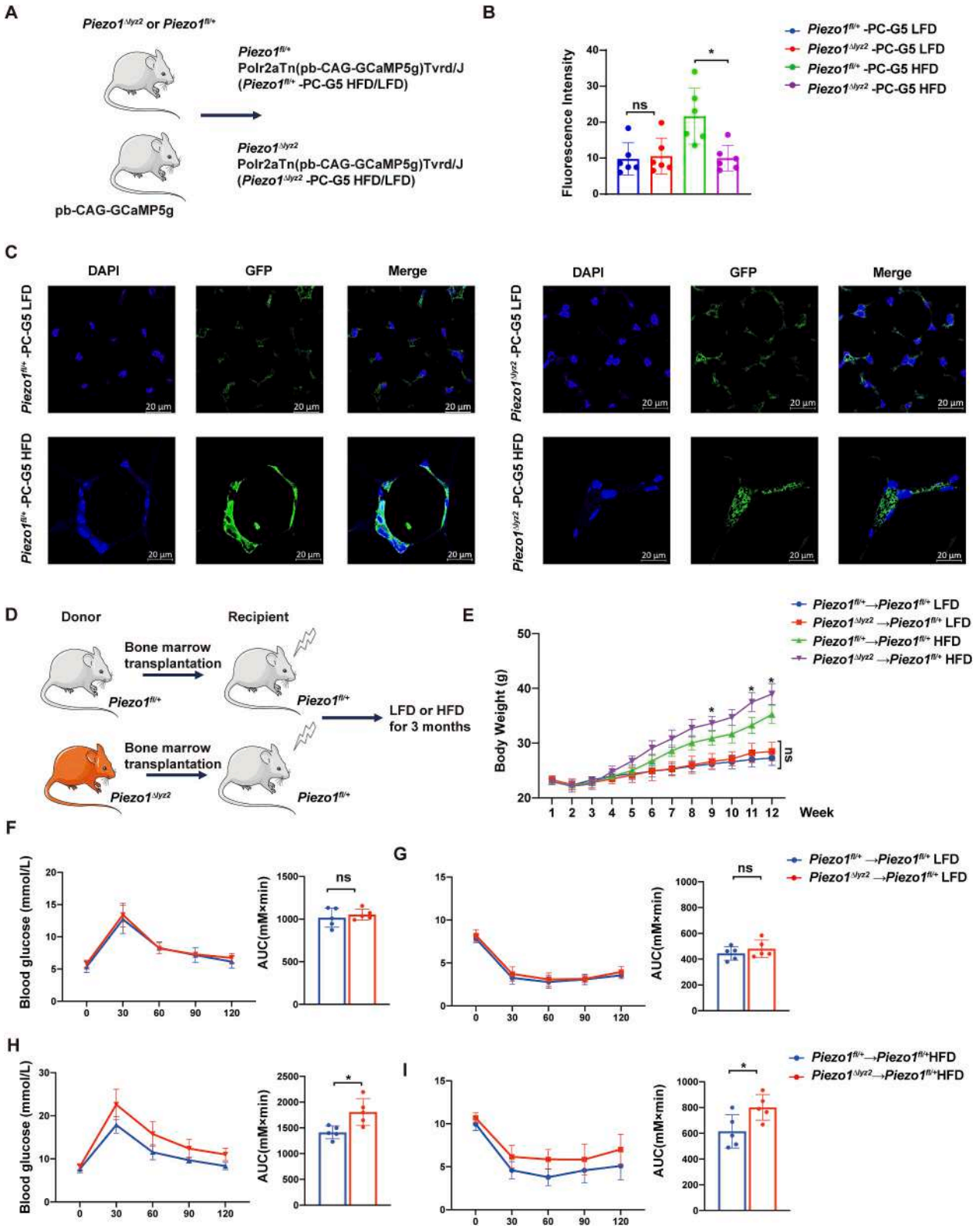

Fig. 3. The adipose tissue macrophages are imperative in body weight regulation with HFD challenge.
(**A**) Schematic diagram outlining the calcium indicator experiment. (**B–C**) Immunofluorescence images of adipose tissue from transgenic reporter mice and quantification of fluorescence intensity. (**D**) Schematic diagram of bone marrow transfer experiment. (**E**) Body weight records of recipient mice exposed to HFD or LFD for 12 weeks ($n = 5$ mice per group). (**F**) Results of GTT for recipient mice on LFD for 12 weeks (n = 5 mice per group). (**G**) Results of ITT for recipient mice on LFD for 12 weeks (n = 5 mice per group). (**H**) GTT results for recipient mice on HFD for 12 weeks (n = 5 mice per group). (**I**) ITT results for recipient mice on HFD for 12 weeks (n = 5 mice per group). Data are expressed as the mean ± SD. Statistical significance was determined using (**E**) two-way ANOVA, $^{*}P < 0.05$, ns = not significant, and (**F–I, B**) two-tailed Student *t*-test, $^{*}P < 0.05$, $^{**}P < 0.01$, ns = not significant.
HFD, high-fat diet; LFD, low-fat diet; GTT, glucose tolerance test; ITT, insulin tolerance test; GFP, green fluorescent protein. (For interpretation of the references to color in this figure legend, the reader is referred to the web version of this article.)

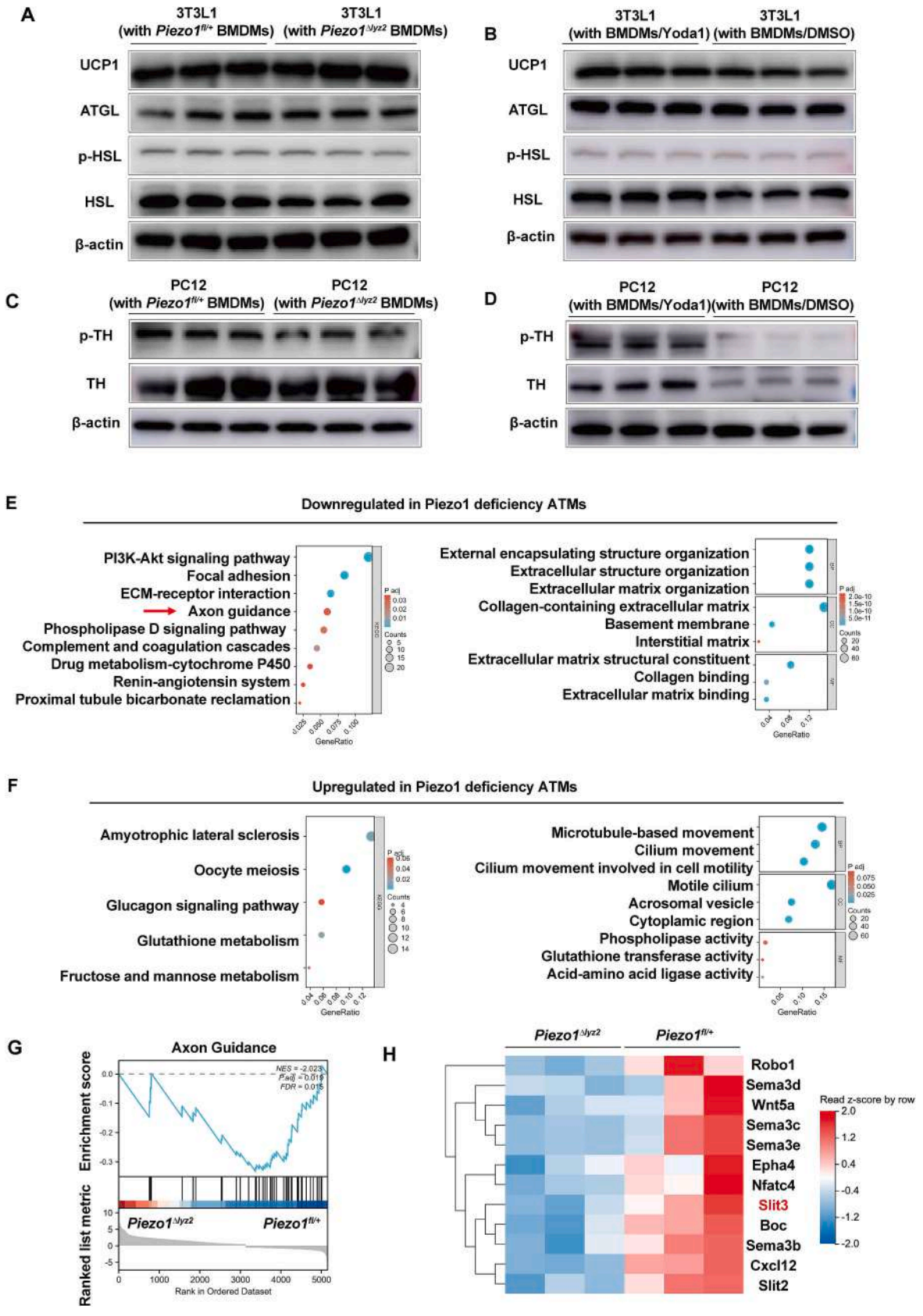

(caption on next page)

Fig. 4. Myeloid Piezo1 regulates weight gain and glucose tolerance in sympathetic activity-dependent pathway.
(**A**) Representative western blot analysis for UCP1, ATGL, p-HSL, and t-HSL in 3T3L1 adipocytes co-cultured with *Piezo1*$^{flox/+}$ and *Piezo1*$^{\Delta lyz2}$ BMDMs. (**B**) Representative western blot analysis for UCP1, ATGL, p-HSL, and t-HSL in 3T3L1 adipocytes with 5 μM Yoda1 treated BMDMs or DMSO-treated BMDMs. (**C**) Representative western blot analysis for p-TH and TH in PC12 cells exposed to conditional medium from *Piezo1*$^{flox/+}$ and *Piezo1*$^{\Delta lyz2}$ BMDMs. (**D**) Representative western blot analysis for p-TH and TH in PC12 cells exposed to conditional medium from 5 μM Yoda1-treated or DMSO-treated BMDMs. (**E**) KEGG pathway enrichment analysis of genes downregulated in KO ATMs (Log2FC > 0.5, Padj<0.05). (**F**) KEGG pathway enrichment analysis of genes upregulated in *Piezo1*$^{\Delta lyz2}$ ATMs (Log2FC > 0.5, Padj<0.05). (**G**) GSEA profiles revealing the axon guidance pathway in ATMs from *Piezo1*$^{flox/+}$ and *Piezo1*$^{\Delta lyz2}$ mice on HFD. (**H**) Heat map illustrating genes in the Axon guidance pathway based on the normalized read count of genes in ATMs from *Piezo1*$^{flox/+}$ and *Piezo1*$^{\Delta lyz2}$ mice on HFD.
HFD, high-fat diet; KEGG, Kyoto Encyclopedia of Genes and Genomes; BMDMs, bone marrow-derived macrophages; GSEA, Gene Set Enrichment Analysis; p-TH, phosphorylated tyrosine hydroxylase.

adipocytes treated with Yoda1 or DMSO-treated BMDMs. UCP1, ATGL, p-HSL, and HSL levels in adipocytes remained unaltered (Fig. 4B, Supplementary Fig. 4B). Hence, we verified that macrophages do not exert their function through direct interactions with adipocytes.

Then we postulated that ATMs indirectly influence adipocytes by affecting sympathetic nerves. PC12 cells treated with the culture supernatant of *Piezo1*$^{\Delta lyz2}$ BMDMs showed a slight tendency to decrease in p-TH (phosphorylated tyrosine hydroxylase)/TH levels (Fig. 4C, Supplementary Fig. 4C). However, the culture supernatant of BMDMs treated with Yoda1 significantly increased p-TH and p-TH/TH in PC12 cells (Fig. 4D, Supplementary Fig. 4D). These results indicate that BMDMs function directly by affecting sympathetic nerves through secreted factors.

To explore how Piezo1 deficiency in macrophages might influence sympathetic activity, subsequently, we isolated ATMs using magnetic bead sorting for F4/80-positive cells in HFD-fed mice and conducted RNA sequencing (RNA-seq). Enrichment analysis revealed potentially altered pathways in Piezo1 deficiency (Fig. 4E, F). Based on evidence that the sympathetic nerve is affected, we noted that RNA-seq experiments on ATMs from *Piezo1*$^{flox/+}$ and *Piezo1*$^{\Delta lyz2}$ mice revealed that differentially expressed genes were enriched in the neuron-related axon guidance pathway in the Kyoto Encyclopedia of Genes and Genomes (KEGG) enrichment analysis. GSEA enrichment profile further confirmed a significant upregulation of this pathway in ATMs from *Piezo1*$^{flox/+}$ mice, with the most differentially expressed genes in this pathway presented in cluster heat maps (Fig. 4G, H). Furthermore, ATMs can reportedly import and degrade NE by expressing Slc6a2 and Maoa, thereby reducing local NE levels [31]. However, neither the RNA-seq cluster heat map of ATMs nor the PCR results indicated altered transcription levels of *Maoa* or *Slc6a2* in *Piezo1*$^{\Delta lyz2}$ mice (Supplementary Fig. 4E, F).

Taken together, we hypothesized that the differential expression of secreted proteins, such as those from the Slit and Sema families, might mediate the neuroregulatory function of ATMs. Slit3 is a key component of the SLIT/ROBO family, acting as a ligand binding to the receptor ROBO1. Among these genes, we focused on Slit3, reportedly secreted by ATMs, and combined with ROBO1 in sympathetic nerves to increase sympathetic activity [32]. We speculated that the activation of Piezo1 in ATMs might enhance the secretion of Slit3 to activate sympathetic nerves.

3.5. Myeloid Piezo1 enhances TH activity in sympathetic nerves by upregulating Slit3 expression

Western blotting and ELISA results revealed that Slit3 expression and secretion in BMDMs increased after Yoda1 treatment (Fig. 5A, B, Supplementary Fig. 5A). Meanwhile, Slit3 levels in medium from *Piezo1*$^{flox/+}$ iWAT were statistically higher than *Piezo1*$^{\Delta lyz2}$ iWAT ($n = 3$ per group) (Fig. 5C). Wang et al. reported that Slit3 secreted from M2-like macrophages increases sympathetic activity and in adipose tissue [32]. Then we visualized gene expression profiles associated with inflammation (Fig. 5D–E). *Piezo1*$^{flox/+}$ ATMs exhibited high expression of several M1-related genes, whereas *Piezo1*$^{\Delta lyz2}$ ATMs displayed elevated expression of M2-related genes. We performed a cytokine array analysis and observed no significant increase in interleukin and chemokine levels in the plasma of HFD-fed *Piezo1*$^{flox/+}$ mice (Fig. 5F). Consequently, we hypothesized that Piezo1 mechanically activates Slit3 secretion independent of polarization.

Then we isolated BMDMs and induced their polarization toward M1 and M2 macrophages with LPS and IL-4, and the Slit3 in the culture supernatant was detected by Elisa. The result showed that Yoda1 can increase the secretion of Slit3, whether in unstimulated *Piezo1*$^{flox/+}$ BMDMs, M1 or M2 (Fig. 5G). The activation effect of Yoda1 can be blocked by Gsmtx4. In addition, Yoda1 did not increase Slit3 secretion in *Piezo1*$^{\Delta lyz2}$ BMDMs.

We validated the Piezo1-induced increase in Slit3 secretion in vitro and further examined whether macrophages in vivo influence sympathetic nerves through the release of Slit3 by performing immunofluorescence assays of adipose tissue sections. First, dual staining of F4/80 and TH revealed that sympathetic nerves (indicated by TH) and macrophages (marked by F4/80) were in close spatial proximity under both lean and obese conditions, establishing a physiological basis for their potential interaction (Supplementary Fig. 5B). Furthermore, Slit3 demonstrated substantial co-localization with macrophages. Under lean conditions, both *Piezo1*$^{flox/+}$ and *Piezo1*$^{\Delta lyz2}$ mice exhibited low Slit3 expression. However, during obesity, *Piezo1*$^{flox/+}$ mice displayed significant elevation of Slit3 expression, whereas *Piezo1*$^{\Delta lyz2}$ mice failed to show such increase (Supplementary Fig. 5C).

Since we confirmed that Yoda1 activated Piezo1 to promote Slit3 release, we then verified the role of Slit3 in obesity induction by transplanting *Piezo1*$^{flox/+}$or *Piezo1*$^{\Delta lyz2}$ bone marrow cells with or without Slit3 knockdown (Fig. 5H). The PCR results show that the knockdown efficiency of Slit3 exceeded 80 % (Supplementary Fig. 5D). After LFD feeding, recipient mice transplanted with *Piezo1*$^{flox/+}$ and *Piezo1*$^{\Delta lyz2}$ bone marrow cells showed no significant differences in body weight, GTT, or ITT, and these parameters remained unchanged after Slit3 knockdown (Supplementary Fig. 5E–G). However, under a high-fat diet, Slit3 knockdown specifically in *Piezo1*$^{flox/+}$ cells recapitulated the phenotype of Piezo1 knockout mice, including increased weight gain and impaired glucose tolerance, whereas Slit3 knockdown in *Piezo1*$^{\Delta lyz2}$ cells did not induce significant alterations (Fig. 5I–K).

3.6. Adaptive thermogenesis enhancement by myeloid Piezo1 is blocked by sympathetic blockade

6-Hydroxydopamine (6-OHDA) is a neurotoxin that selectively destroys catecholaminergic nerves in sympathetically innervated tissues and has been widely used to create animal models of Parkinson's disease [49]. To confirm that Piezo1-deficient macrophages regulate the development of obesity by affecting sympathetic nerve activity and influencing adaptive thermogenesis, we locally injected 6-OHDA into bilateral fat pads for local sympathetic denervation. This injection significantly reduced the body weight difference between *Piezo1*$^{flox/+}$ and *Piezo1*$^{\Delta lyz2}$ groups specifically under a high-fat diet (Fig. 6A, B). Importantly, no notable difference in body weight was observed between *Piezo1*$^{flox/+}$ and *Piezo1*$^{\Delta lyz2}$ mice on a low-fat diet, regardless of the intervention (Supplementary Fig. 6A). Notably, the rectal temperature difference under cold stimulation was significantly attenuated following 6-OHDA intervention, irrespective of whether the mice were on a high-fat or low-fat diet (Fig. 6C, Supplementary Fig. 6B). We

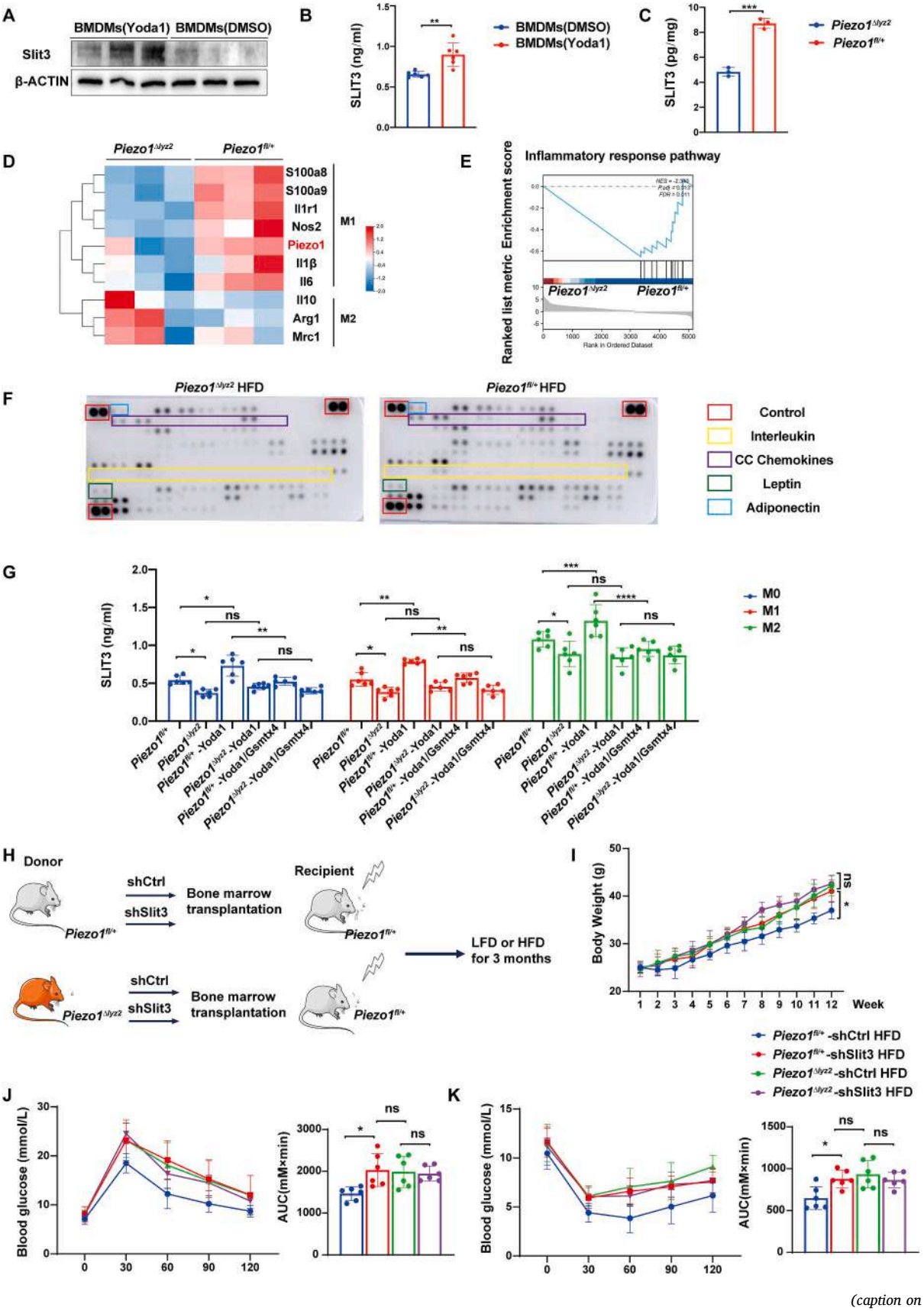

(caption on next page)

Fig. 5. Myeloid Piezo1 enhances TH activity in sympathetic nerves by upregulating Slit3 expression.
(**A**) Western blot analysis for Slit3 in BMDMs treated with 5 μM Yoda1 or DMSO for 24 h. (**B**) Slit3 secretion by BMDMs treated with 5 μM Yoda1 or DMSO for 24 h. (**C**) Slit3 levels in medium from iWAT isolated from *Piezo1*$^{flox/+}$ and *Piezo1*$^{\Delta lyz2}$ mice with HFD fed ($n = 3$ per group). (**D**) Heat map illustrating inflammation-related genes based on the normalized read count of genes in ATMs from *Piezo1*$^{flox/+}$ and *Piezo1*$^{\Delta lyz2}$ mice fed with HFD. (**E**) GSEA profiles revealing the inflammatory response pathway in ATMs from *Piezo1*$^{flox/+}$ and *Piezo1*$^{\Delta lyz2}$ mice on HFD. (**F**) Cytokine array images of serum cytokine/chemokine of HFD-*Piezo1*$^{flox/+}$ mice and HFD-*Piezo1*$^{\Delta lyz2}$ mice. (**G**) Slit3 levels in supernatant from M0, M1 and M2 BMDMs by Elisa ($n = 6$). (**H**) Schematic diagram of bone marrow transplantation with or without Slit3 interference. (**I**) Body weight records of recipient mice exposed to HFD for 12 weeks (n = 6 mice per group). (**J**) Results of GTT for recipient mice on HFD for 12 weeks (n = 6 mice per group). (**K**) Results of ITT for recipient mice on HFD for 12 weeks (n = 6 mice per group). Statistical significances were calculated using (**B, C**) two-tailed Student t-test, (**I**) two-way ANOVA, (**G, J, K**) one-way ANOVA and Tukey's multiple comparisons test. Data are expressed as the mean ± SD. $^*P < 0.05$, $^{**}P < 0.01$, $^{***}P < 0.001$; $^{****}P < 0.0001$, ns = not significant.
HFD, high-fat diet; LFD, low-fat diet; ATMs, adipose tissue macrophages; GTT, glucose tolerance test; ITT, insulin tolerance test; GSEA, Gene Set Enrichment Analysis.

hypothesize that the localized elevation of NE levels induced by cold exposure may have amplified this physiological discrepancy. 6-OHDA treatment significantly inhibited the expression of p-TH, TH, and lipid metabolism-related proteins during obesity (Fig. 6D, Supplementary Fig. 6C). Immunohistochemical analysis revealed a considerable inhibition of UCP1 and TH expression (Fig. 6E). These results suggested that the function of Piezo1 depends on sympathetic activity.

Since immune cells also partially express NE receptors but have been confirmed to lack TH expression, we selected a tyrosine hydroxylase inhibitor, α-methyl-p-tyrosine (αMPT) for local adipose tissue injection to more precisely verify the critical role of sympathetic nerves in this process. We then measured short-term body weight changes in *Piezo1*$^{flox/+}$ and *Piezo1*$^{\Delta lyz2}$ mice under HFD and LFD conditions. The results showed remarkable similarity to those from 6-OHDA administration: local αMPT administration also eliminated the differences in weight gain and cold tolerance between *Piezo1*$^{flox/+}$ and *Piezo1*$^{\Delta lyz2}$ mice on HFD (Supplementary Fig. 6D–F). Collectively, the experimental results from both αMPT and 6-OHDA indicate that the effect of Piezo1 on body weight regulation is sympathetic nerve-dependent.

To further confirm the role of the Slit3–ROBO1 axis in the function of Piezo1 in ATMs, we locally injected shROBO1 or shCtrl solution into bilateral fat pads. ROBO1 knockdown produced effects similar to that of 6-OHDA treatment in HFD-fed mice. shROBO1 injection reduced variations in body weight, rectal temperature under cold stimulation between *Piezo1*$^{flox/+}$ and *Piezo1*$^{\Delta lyz2}$ mice (Fig. 6F–H). shROBO1 significantly inhibited the expression of p-TH, TH, and lipid metabolism-related proteins (Fig. 6I, Supplementary Fig. 6H). Immunohistochemical analysis revealed considerable inhibition of UCP1 and TH expression upon shROBO1 treatment (Fig. 6J). These results suggest that the Slit3–ROBO1 pathway is indispensable for the neuroregulatory function of Piezo1 in ATMs in vivo.

To dissect the macrophage-autonomous role of ROBO1, we transplanted shROBO1 -treated *Piezo1*$^{flox/+}$ or *Piezo1*$^{\Delta lyz2}$ bone marrow cells into recipient mice, followed by dietary challenge (LFD or HFD), thereby directly testing the necessity of macrophage-intrinsic Robo1 signaling in obesity pathogenesis (Supplementary Fig. 7A). The results demonstrated that, following bone marrow cell transplantation, recipient mice under LFD conditions showed no significant differences in body weight or glucose tolerance, consistent with our previous findings (Supplementary Fig. 7B, D, E). However, under HFD challenge, *Piezo1*$^{\Delta lyz2}$ cell-transplanted mice exhibited markedly increased body weight and more severe glucose tolerance impairment (Supplementary Fig. 7C). Critically, Robo1 interference in macrophages failed to induce discernible phenotypic alterations under HFD-fed (Supplementary Fig. 7F-G). This finding suggests that Slit3-mediated regulation does not operate through macrophage-autonomous autocrine signaling loops.

3.7. Piezo1 activates Slit3 expression through the transcription factor SP1 in BMDMs

To further explore the molecular mechanism by which Piezo1 promotes the expression and secretion of Slit3, transcription factor prediction was performed to identify the possible transcription factors that regulate Slit3 expression based on multiple transcription factor databases. Seven candidates, JUND, STAT1, YY1, RELA, PAX5, POU5F1 and SP1 were identified via a Venn diagram approach (Fig. 7A). That is, these seven candidates were found at the intersection of all the sets in the Venn diagram and might mediate the expression of Slit3. Therefore, we used small interfering RNA (siRNA) of these seven transcription factors and verified the interference efficiency (Supplementary Fig. 6I). After adding Yoda1 and different siRNA to BMDMs, we examined Slit3 expression and found that suppression of SP1 significantly reduced Slit3 expression (Fig. 7B). In addition, Yoda1 can increase the SP1 transportation to the nucleus in BMDMs (Fig. 7C, Supplementary Fig. 6J). At the protein level, inhibition of SP1 could inhibit the secretion of Slit3 stimulated by Yoda1(Fig. 7D). We verified that Yoda1 increases SP1 binding in the Slit3 promoter region by Chip-qPCR (Fig. 7E). Furthermore, our in vivo RNA-seq data revealed that other downstream genes transcriptionally regulated by SP1 exhibited consistent trends with Slit3 (Fig. 7F), further confirming that SP1 is regulated by Piezo1-mediated mechanosensory signaling. These findings suggested that SP1 plays an important role in the effect of the Piezo1 in promoting the Slit3 expression in BMDMs.

4. Discussion

In this study, we demonstrated that Piezo1-dependent mechanosensation in ATMs enhances the secretion of Slit3 by activating transcription factor SP1 during obesity. Consequently, Slit3 plays a crucial role in promoting the synthesis and release of NE in sympathetic neurons by binding to the ROBO1 receptor and facilitating the phosphorylation of TH. This cascade of events leads to improved lipolysis and heat production, ultimately limiting the progression of obesity. These findings suggest that Piezo1 in ATMs mediate a negative feedback mechanism. As obesity develops, an increased number of ATMs accumulate in adipose tissue, and these mechano-activated ATMs promote NE secretion and thermogenesis, contributing to the maintenance of energy homeostasis and body temperature. However, specific knockout of Piezo1 disrupts this negative feedback loop, exacerbating the imbalance between energy storage and expenditure in obese mice.

Thermogenesis has long been associated with BAT. However, exposure to cold triggers the infiltration of ATMs into subcutaneous WAT via CCR2 [50] and HFD also promotes the recruitment of ATMs to infiltrate visceral WAT [51], emphasizing the crucial role of WAT ATMs in regulating energy expenditure, particularly thermogenesis. Our findings suggest that accumulated and Piezo1-activated ATMs in WAT may promote thermogenesis in a NE-dependent manner. This sheds light on the pivotal role of infiltrated ATMs in adipocyte thermogenesis. NE, secreted by sympathetic nerve terminals, serves as a central and well-studied hormone governing ligand-mediated adaptive and facultative adipocyte thermogenesis [52]. While previous research has predominantly focused on β-adrenergic receptor (β-AR) signaling and UCP1 expression in NE-mediated thermogenesis [53,54], our findings indicate a decreased expression of UCP1 in both WAT and BAT of HFD-challenged *Piezo1*$^{\Delta lyz2}$ mice. This confirms the involvement of Piezo1 in ATMs in the thermoregulatory network.

M1 macrophages are key contributors to chronic inflammation and insulin resistance in HFD-induced obese mice. Selective deletion of

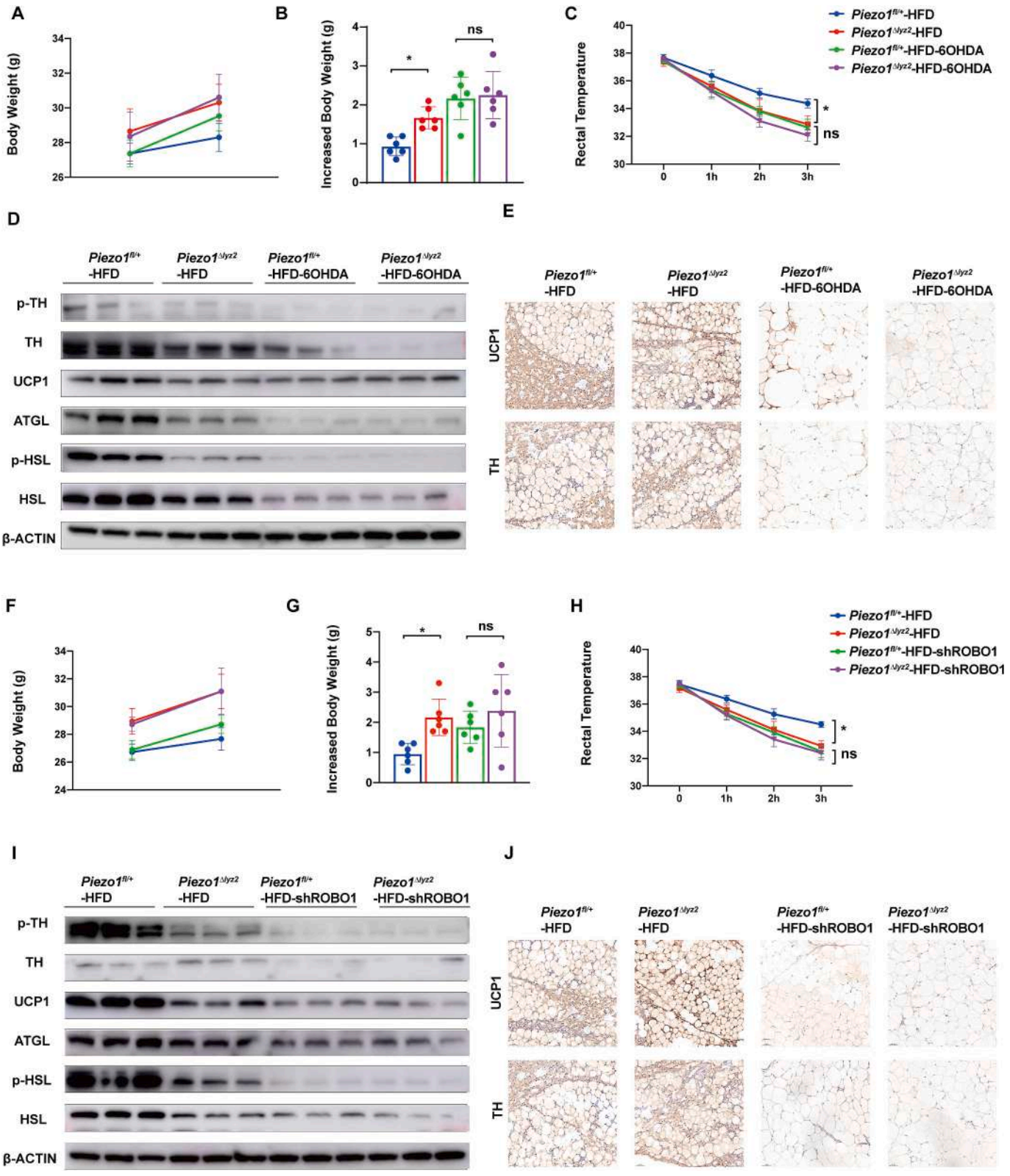

Fig. 6. Adaptive thermogenesis enhancement by myeloid Piezo1 is blocked by sympathetic blockade.
(**A**) Body weight records, (**B**) increased body weight analysis, (**C**) rectal temperature measurements under cold challenge. (**D**) representative western blot analysis, and (**E**) representative immunohistochemical images of *Piezo1*$^{flox/+}$ and *Piezo1*$^{\Delta lyz2}$ mice challenged with HFD with or without bilateral fat pad injection of 6-OHDA (6-Hydroxydopamine) (200 μg per lobe) for 7 days (n = 6 mice per group). (**F**) Body weight records, (**G**) increased body weight analysis, (**H**) rectal temperature measurements under cold challenge. (**I**) representative western blot analysis, and (**J**) representative immunohistochemical images of WAT from *Piezo1*$^{flox/+}$ and *Piezo1*$^{\Delta lyz2}$ mice challenged with HFD with shROBO1 or shCtrl injected bilaterally into the fat pad three times a week (n = 6 mice per group). Data are expressed as the mean ± SD. Statistical significances were determined using (**C, H**) two-way ANOVA and (**B, G**) one-way ANOVA and Tukey's multiple comparisons test. *P < 0.05, ns = not significant.
NE, norepinephrine; HFD, high-fat diet; 6-OHDA, 6-hydroxydopamine.

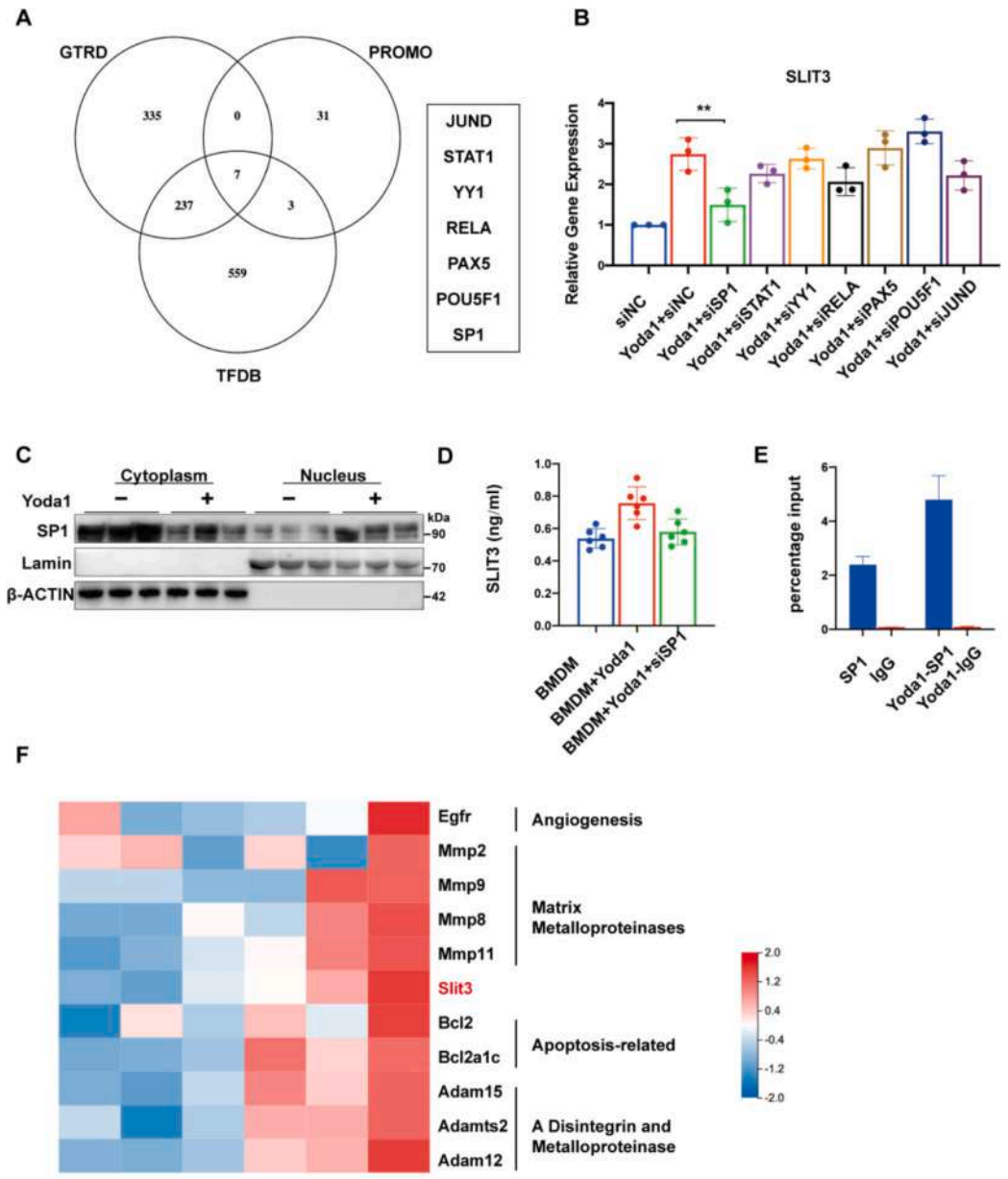

Fig. 7. Piezo1 activates Slit3 expression through the transcription factor SP1 in BMDMs (**A**) Venn diagram showing the possible target transcription factor of Slit3 by three online databases (i.e., GTRD, TFDB and PROMO). (**B**) qRT-PCR analysis of Slit3 after transfected with small interfering RNA of different transcription factors in BMDMs. (**C**) Representative western blot analysis for SP1 in BMDMs with or with not Yoda1 in medium. (**D**) Elisa analysis for Slit3 in BMDMs exposed to Yoda1 or with SP1 knock-down. (**E**) The SP1 antibody was used for Chip-qPCR test, the Slit3 promoter sequence was designed by primer, and the enriched DNA was detected by qPCR in BMDMs with or without Yoda1. (**F**) Heat map illustrating SP1-related genes based on the normalized read count of genes in ATMs from *Piezo1*$^{flox/+}$ and *Piezo1*$^{\Delta lyz2}$ mice fed with HFD. Statistical significances were calculated using (**B, D**) one-way ANOVA and Tukey's multiple comparisons test. Data are expressed as the mean ± SD. *P < 0.05, **P < 0.01, ***P < 0.001; **** P < 0.0001, ns = not significant.

CD11c^{+} M1 macrophages through the administration of diphtheria toxin, with the diphtheria toxin receptor expressed under the control of the CD11c promoter in obese mice, leads to improved insulin sensitivity and reduced inflammatory markers [55]. TNF-α and the pro-inflammatory lectin Galectin-3, secreted by M1 macrophages, can inhibit insulin-stimulated glucose uptake in adipocytes [56,57]. Activation of Piezo1 in macrophages can upregulate the expression of pro-inflammatory M1-related genes induced by interferon-γ (IFN-γ) or lipopolysaccharide (LPS) while suppressing the expression of IL-4- and IL-13-induced anti-inflammatory M2-related genes [37]. Thus, we initially speculated that Piezo1 deficiency in ATMs would reduce inflammation and mitigate obesity. Counterintuitively, Piezo1 deficiency in ATMs resulted in increased body weight and the development of insulin resistance in obese mice, despite the lower expression of pro-inflammatory M1-related genes and higher expression of anti-inflammatory M2-related genes in Piezo1-deficient ATMs. Our validation using 6-OHDA and shROBO1 validates that Piezo1-activated ATMs can modulate NE-dependent thermogenesis in obese mice, exerting a more pronounced effect than inflammatory cytokines on energy balance. This unexpected outcome may also be partly attributed to the chronic low-grade systemic inflammation characterizing obesity [58], which differs from acute systemic immune responses such as infection or tissue damage, where the inflammation-regulatory function of Piezo1 may not prevail in the HFD-induced mouse model.

The relationship between macrophages and the sympathetic nervous system remains a topic of debate. While some researchers have posited

that M2 ATMs in WAT can directly produce NE to promote thermogenesis [59], Katrin Fischer et al. proposed an opposing viewpoint. Through the generation of mice with a specific absence of TH in macrophages, they established that the absence of TH in myeloid cells does not impact adaptive thermogenesis in mice [43]. Consequently, the prevailing consensus is that macrophages do not directly regulate thermogenesis by producing NE. Notably, Pirzgalska Roksana M et al. identified a novel subset of sympathetically associated macrophages (SAMs) that functionally regulate thermogenesis through MAOA and the norepinephrine transporter, SLC6A2, mediating the clearance of extracellular NE [31]. Our findings helped exclude the possibility that Piezo1 activation may regulate the expression of MAOA and SLC6A2. Furthermore, M2 macrophages have been shown to stimulate sympathetic innervation in mice by secreting Slit3. However, the dynamic regulation of Slit3 secretion by the altered microenvironment in adipose tissue during obesity remains unknown. Here, we observed that Piezo1 activation significantly enhances the expression and secretion of Slit3, suggesting that Slit3 may serve as a novel mechanosensitive signal in ATMs.

Regarding the neurotransmitters of the sympathetic nervous system, we have thoroughly evaluated the potential interference of epinephrine (adrenaline) on experimental outcomes. It is important to note that both epinephrine and NE play roles in mobilizing lipid metabolism during stress responses [60]. However, the synthesis of epinephrine critically depends on phenylethanolamine *N*-methyltransferase (PNMT), whose expression relies on cortisol secreted by the adrenal cortex [61,62]. Consequently, epinephrine is primarily synthesized in the adrenal medulla rather than peripheral tissues, exerting systemic effects through circulatory distribution [63]. In contrast, NE is mainly secreted by sympathetic nerve terminals for local sympathetic regulation [64]. Previous studies have demonstrated that sympathetic nerve blockade effectively inhibits lipid mobilization in adipose tissue, whereas adrenal demedullation fails to produce such effects [65–68]. Our findings corroborate this by showing undetectably low levels of epinephrine in local adipose tissue, with significant differences observed specifically in NE levels between *Piezo1*$^{flox/+}$ and *Piezo1*$^{\Delta lyz2}$ mice. These results underscore the pivotal role of sympathetic nerve-derived NE in maintaining adipose tissue homeostasis.

Collectively, our findings suggest that the activation of Piezo1 enhances the expression and secretion of Slit3, which subsequently acts on the ROBO1 receptor in sympathetic neurons. This activation promotes sympathetic nerve activity and augments adaptive thermogenesis in mice. This mechanosensitive signaling pathway not only advances our understanding of mechanosensation in obesity but also offers potential targets for future mechano-therapeutic strategies aimed at mitigating obesity and type 2 diabetes.

CRediT authorship contribution statement

Shaoqiu Leng: Writing – review & editing, Writing – original draft, Visualization, Validation, Supervision, Software, Resources, Project administration, Methodology, Investigation, Funding acquisition, Formal analysis, Data curation, Conceptualization. **Xiaoyu Zhang:** Writing – review & editing, Writing – original draft, Visualization, Methodology, Investigation, Funding acquisition, Formal analysis, Data curation, Conceptualization. **Ruxia Zhao:** Writing – review & editing, Writing – original draft, Project administration, Methodology, Investigation, Funding acquisition, Formal analysis, Data curation, Conceptualization. **Nan Jiang:** Writing – original draft, Validation, Supervision, Software, Methodology. **Xinyue Liu:** Supervision, Software, Methodology. **Xin Li:** Supervision, Software, Resources. **Qi Feng:** Resources, Project administration, Methodology. **Zi Sheng:** Software, Resources. **Shuwen Wang:** Writing – review & editing, Writing – original draft, Visualization, Project administration, Methodology, Formal analysis, Data curation, Conceptualization. **Jun Peng:** Writing – review & editing, Writing – original draft, Visualization, Validation, Supervision, Methodology, Investigation, Formal analysis, Data curation, Conceptualization. **Xiang Hu:** Writing – review & editing, Writing – original draft, Visualization, Validation, Supervision, Software, Resources, Project administration, Methodology, Investigation, Funding acquisition, Formal analysis, Data curation, Conceptualization.

Funding

This work was supported by grants from the National Natural Science Foundation of China (No. 82030005, 82200138, 82170124 and 82270130), National Key Research and Development Program of China (No. 2023YFC2507800), Taishan Scholar Foundation of Shandong Province (No. ts20221157 and tsqn202306350), Natural Science Foundation of Shandong Province (No. ZR2022QH081), Postdoctoral Innovation Project of Shandong Province (No. SDCX-ZG-202302029), China Postdoctoral Science Foundation (No. 2023M732098), Clinical research project of Shandong University (No. 2021SDUCRCB008) and Cutting Edge Development Fund of Advanced Medical Research Institute.

Declaration of competing interest

The authors declare that they have no conflict of interest.

Acknowledgments

The authors thank Translational Medicine Core Facility of Shandong University for consultation and instrument availability that supported this work. The graphical abstract was completed in Figdraw (www.figdraw.com).

Appendix A. Supplementary data

Supplementary data to this article can be found online at https://doi.org/10.1016/j.metabol.2025.156262.

Data availability

All datasets generated and/or analyzed during the current study are available from the corresponding authors. Raw data have been deposited to National Center for Biotechnology Information (NCBI) under the BioProject number PRJNA1242553.

References

[1] Haslam DW, James WP. Obesity. Lancet 2005;366(9492):1197–209.
[2] Watanabe K, et al. Multiomic signatures of body mass index identify heterogeneous health phenotypes and responses to a lifestyle intervention. Nat. Med. 2023;29(4):996–1008.
[3] Godfrey KM, et al. Influence of maternal obesity on the long-term health of offspring. Lancet Diabetes Endocrinol 2017;5(1):53–64.
[4] Wang Y, et al. Prevention and control of obesity in China. Lancet Glob Health 2019;7(9):e1166–7.
[5] Wen X, et al. Signaling pathways in obesity: mechanisms and therapeutic interventions. Signal Transduct Target Ther 2022;7(1):298.
[6] Fisher FM, et al. FGF21 regulates PGC-1α and browning of white adipose tissues in adaptive thermogenesis. Genes Dev 2012;26(3):271–81.
[7] Senthivinayagam S, et al. Adaptive thermogenesis in brown adipose tissue involves activation of pannexin-1 channels. Mol Metab 2021;44:101130.
[8] Golozoubova V, et al. Only UCP1 can mediate adaptive nonshivering thermogenesis in the cold. FASEB J 2001;15(11):2048–50.
[9] Zhang L, et al. Diet-induced adaptive thermogenesis requires neuropeptide FF receptor-2 signalling. Nat Commun 2018;9(1):4722.
[10] Yamamoto Y, et al. Adipose depots possess unique developmental gene signatures. Obesity (Silver Spring) 2010;18(5):872–8.
[11] Lehnig AC, Stanford KI. Exercise-induced adaptations to white and brown adipose tissue. J Exp Biol 2018;221(Pt Suppl 1).
[12] Lim S, et al. Cold-induced activation of brown adipose tissue and adipose angiogenesis in mice. Nat Protoc 2012;7(3):606–15.
[13] Whitehead A, et al. Brown and beige adipose tissue regulate systemic metabolism through a metabolite interorgan signaling axis. Nat Commun 2021;12(1):1905.

[14] Stine RR, et al. EBF2 promotes the recruitment of beige adipocytes in white adipose tissue. Mol Metab 2016;5(1):57–65.
[15] Brestoff JR, et al. Group 2 innate lymphoid cells promote beiging of white adipose tissue and limit obesity. Nature 2015;519(7542):242–6.
[16] Maniyadath B, et al. Adipose tissue at single-cell resolution. Cell Metab 2023;35(3):386–413.
[17] Chouchani ET, Kazak L, Spiegelman BM. New advances in adaptive thermogenesis: UCP1 and beyond. Cell Metab 2019;29(1):27–37.
[18] Fedorenko A, Lishko PV, Kirichok Y. Mechanism of fatty-acid-dependent UCP1 uncoupling in brown fat mitochondria. Cell 2012;151(2):400–13.
[19] Shi M, et al. AIDA directly connects sympathetic innervation to adaptive thermogenesis by UCP1. Nat Cell Biol 2021;23(3):268–77.
[20] Xue K, et al. The mitochondrial calcium uniporter engages UCP1 to form a thermoporter that promotes thermogenesis. Cell Metab 2022;34(9):1325–1341.e6.
[21] Yao J, Wu D, Qiu Y. Adipose tissue macrophage in obesity-associated metabolic diseases. Front Immunol 2022;13:977485.
[22] Lumeng CN, Bodzin JL, Saltiel AR. Obesity induces a phenotypic switch in adipose tissue macrophage polarization. J Clin Invest 2007;117(1):175–84.
[23] Zhuge F, et al. DPP-4 inhibition by Linagliptin attenuates obesity-related inflammation and insulin resistance by regulating M1/M2 macrophage polarization. Diabetes 2016;65(10):2966–79.
[24] Huh JH, et al. Dual CCR2/5 antagonist attenuates obesity-induced insulin resistance by regulating macrophage recruitment and M1/M2 status. Obesity (Silver Spring) 2018;26(2):378–86.
[25] Fujisaka S, et al. Regulatory mechanisms for adipose tissue M1 and M2 macrophages in diet-induced obese mice. Diabetes 2009;58(11):2574–82.
[26] Lin S, et al. Targeting parvalbumin promotes M2 macrophage polarization and energy expenditure in mice. Nat Commun 2022;13(1):3301.
[27] Xu L, Ota T. Emerging roles of SGLT2 inhibitors in obesity and insulin resistance: focus on fat browning and macrophage polarization. Adipocyte 2018;7(2):121–8.
[28] Phu TA, et al. IL-4 polarized human macrophage exosomes control cardiometabolic inflammation and diabetes in obesity. Mol Ther 2022;30(6):2274–97.
[29] Kim J, et al. TFEB-GDF15 axis protects against obesity and insulin resistance as a lysosomal stress response. Nat Metab 2021;3(3):410–27.
[30] Man K, Kallies A, Vasanthakumar A. Resident and migratory adipose immune cells control systemic metabolism and thermogenesis. Cell Mol Immunol 2022;19(3):421–31.
[31] Pirzgalska RM, et al. Sympathetic neuron-associated macrophages contribute to obesity by importing and metabolizing norepinephrine. Nat Med 2017;23(11):1309–18.
[32] Wang YN, et al. Slit3 secreted from M2-like macrophages increases sympathetic activity and thermogenesis in adipose tissue. Nat Metab 2021;3(11):1536–51.
[33] Kawai T, Autieri MV, Scalia R. Adipose tissue inflammation and metabolic dysfunction in obesity. Am J Physiol Cell Physiol 2021;320(3):C375–c391.
[34] Chen HJ, et al. Adipose extracellular matrix deposition is an indicator of obesity and metabolic disorders. J Nutr Biochem 2023;111:109159.
[35] Geng J, et al. TLR4 signalling via Piezo1 engages and enhances the macrophage mediated host response during bacterial infection. Nat Commun 2021;12(1):3519.
[36] Saotome K, et al. Structure of the mechanically activated ion channel Piezo1. Nature 2018;554(7693):481–6.
[37] Atcha H, et al. Mechanically activated ion channel Piezo1 modulates macrophage polarization and stiffness sensing. Nat Commun 2021;12(1):3256.
[38] Zhao Q, et al. Structure and mechanogating mechanism of the Piezo1 channel. Nature 2018;554(7693):487–92.
[39] Wang S, et al. Adipocyte Piezo1 mediates obesogenic adipogenesis through the FGF1/FGFR1 signaling pathway in mice. Nat Commun 2020;11(1):2303.
[40] Zhao C, et al. Mechanosensitive Ion channel Piezo1 regulates diet-induced adipose inflammation and systemic insulin resistance. Front Endocrinol (Lausanne) 2019;10:373.
[41] Leng S, et al. Ion channel Piezo1 activation promotes aerobic glycolysis in macrophages. Front Immunol 2022;13:976482.
[42] Hildreth AD, et al. Single-cell sequencing of human white adipose tissue identifies new cell states in health and obesity. Nat Immunol 2021;22(5):639–53.
[43] Fischer K, et al. Alternatively activated macrophages do not synthesize catecholamines or contribute to adipose tissue adaptive thermogenesis. Nat Med 2017;23(5):623–30.
[44] Russo L, Lumeng CN. Properties and functions of adipose tissue macrophages in obesity. Immunology 2018;155(4):407–17.
[45] Kim J, et al. Silencing CCR2 in macrophages alleviates adipose tissue inflammation and the associated metabolic syndrome in dietary obese mice. Mol Ther Nucleic Acids 2016;5(1):e280.
[46] Weisberg SP, et al. CCR2 modulates inflammatory and metabolic effects of high-fat feeding. J Clin Invest 2006;116(1):115–24.
[47] Blériot C, Chakarov S, Ginhoux F. Determinants of resident tissue macrophage identity and function. Immunity 2020;52(6):957–70.
[48] Ginhoux F, et al. Single-cell immunology: past, present, and future. Immunity 2022;55(3):393–404.
[49] Simola N, Morelli M, Carta AR. The 6-hydroxydopamine model of Parkinson's disease. Neurotox Res 2007;11(3–4):151–67.
[50] Qiu Y, et al. Eosinophils and type 2 cytokine signaling in macrophages orchestrate development of functional beige fat. Cell 2014;157(6):1292–308.
[51] Wensveen FM, et al. The "big bang" in obese fat: events initiating obesity-induced adipose tissue inflammation. Eur J Immunol 2015;45(9):2446–56.
[52] Hsieh AC, Carlson LD. Role of adrenaline and noradrenaline in chemical regulation of heat production. Am J Physiol 1957;190(2):243–6.
[53] Cero C, et al. β3-Adrenergic receptors regulate human brown/beige adipocyte lipolysis and thermogenesis. JCI. Insight 2021;6(11).
[54] Blondin DP, et al. Human Brown adipocyte thermogenesis is driven by β2-AR stimulation. Cell Metab 2020;32(2):287–300.e7.
[55] Patsouris D, et al. Ablation of CD11c-positive cells normalizes insulin sensitivity in obese insulin resistant animals. Cell Metab 2008;8(4):301–9.
[56] Suganami T, Nishida J, Ogawa Y. A paracrine loop between adipocytes and macrophages aggravates inflammatory changes: role of free fatty acids and tumor necrosis factor alpha. Arterioscler Thromb Vasc Biol 2005;25(10):2062–8.
[57] Li P, et al. Hematopoietic-derived Galectin-3 causes cellular and systemic insulin resistance. Cell 2016;167(4):973–984.e12.
[58] Solinas G. Molecular pathways linking metabolic inflammation and thermogenesis. Obes Rev 2012;13(Suppl. 2):69–82.
[59] Nguyen KD, et al. Alternatively activated macrophages produce catecholamines to sustain adaptive thermogenesis. Nature 2011;480(7375):104–8.
[60] Kvetnansky R, Sabban EL, Palkovits M. Catecholaminergic systems in stress: structural and molecular genetic approaches. Physiol Rev 2009;89(2):535–606.
[61] Baetge EE, et al. Transgenic mice express the human phenylethanolamine N-methyltransferase gene in adrenal medulla and retina. Proc Natl Acad Sci U S A 1988;85(10):3648–52.
[62] Wong DL, et al. Glucocorticoid regulation of phenylethanolamine N-methyltransferase in vivo. FASEB J 1992;6(14):3310–5.
[63] Kvetnansky R, et al. Effects of chronic guanethidine treatment and adrenal medullectomy on plasma levels of catecholamines and corticosterone in forcibly immobilized rats. J Pharmacol Exp Ther 1979;209(2):287–91.
[64] Syková E. Extrasynaptic volume transmission and diffusion parameters of the extracellular space. Neuroscience 2004;129(4):861–76.
[65] Lazzarini SJ, Wade GN. Role of sympathetic nerves in effects of estradiol on rat white adipose tissue. Am J Physiol 1991;260(1 Pt 2):R47–51.
[66] Demas GE. Splenic denervation blocks leptin-induced enhancement of humoral immunity in Siberian hamsters (Phodopus sungorus). Neuroendocrinology 2002;76(3):178–84.
[67] Youngstrom TG, Bartness TJ. White adipose tissue sympathetic nervous system denervation increases fat pad mass and fat cell number. Am J Physiol 1998;275(5):R1488–93.
[68] Takahashi A, Shimazu T. Hypothalamic regulation of lipid metabolism in the rat: effect of hypothalamic stimulation on lipolysis. J Auton Nerv Syst 1981;4(3):195–205.